Journal of Nanotechnology

WILEY

RESEARCH ARTICLE OPEN ACCESS

The Effect of Foliar Nano CeO_2/SiO_2 Fertilizer on the Growth of *Salvia miltiorrhiza* Bunge and *Paramignya trimera* (Oliv.) Guillaume

Cao Van Hoang[1] | Nguyen Vu Ngoc Mai[1] | Nguyen Thi Dieu Cam[1] | Vo Van Duyen Em[2] | Nguyen Viet Trung[2] | Dang Thi Ngoc Hoa[3] | Nguyen Thi Thu Phuong[4,5] | Nguyen Chi Bao[6] | Ho Van Minh Hai[5] | Le Thi Hoa[5] | Nguyen Hai Phong[5] | Dinh Quang Khieu[5]

[1]Faculty of Natural Science, Quy Nhon University, Quy Nhon, Gia Lai, Vietnam | [2]Faculty of Education, Quy Nhon University, Quy Nhon, Gia Lai, Vietnam | [3]University of Medicine and Pharmacy, Hue University, Hue city, Vietnam | [4]Thuan Hoa High School, University of Education, Hue University, Hue, Vietnam | [5]University of Sciences, Hue University, Hue, Vietnam | [6]Hue University, Hue, Vietnam

Correspondence: Cao Van Hoang (caovanhoang@qnu.edu.vn) | Nguyen Thi Thu Phuong (nttphuong.dhkh24@hueuni.edu.vn) | Dinh Quang Khieu (dqkhieu@hueuni.edu.vn)

Received: 25 May 2025 | **Revised:** 1 March 2026 | **Accepted:** 20 April 2026

Academic Editor: Virat Khanna

Keywords: CeO_2/SiO_2nanoparticles | Co-60 gamma | *Paramignya trimera* (Oliv.) Guillaume | *Salvia miltiorrhiza* Bunge

ABSTRACT

In the present work, CeO_2/SiO_2 nanoparticles (CeO_2/SiO_2 NPs) were synthesized using a Co-60 gamma irradiation-assisted green method, utilizing rice husk-derived SiO_2, cerium salt, and 2% chitosan as a stabilizing matrix. The resulting nanoparticles were well dispersed in the chitosan matrix, with an average size of 12.6 ± 2.5 nm. The process is scalable at the pilot level and environmentally friendly. A 12-month pot experiment was conducted to evaluate the biostimulatory effects of CeO_2/SiO_2 NPs on *Salvia miltiorrhiza* Bunge (SMB) and *Paramignya trimera* (Oliv.) Guillaume (PTG). In SMB, treated plants exhibited increased growth parameters, with chlorophyll B reaching 26.1 $\mu g\ g^{-1}$ at 12 months—about 13% higher than the control. At an optimal concentration of 2.0 $g\ L^{-1}$, seed sprouting increased from 14% to 34%, shoot height from 2.0 to 9.5 cm, root length from 11.0 to 22.5 cm, and root number from 5.4 to 11.9. In PTG, CeO_2/SiO_2 treatment significantly improved vegetative growth and enhanced the accumulation of key bioactive compounds, including ostruthin, 8-methoxyostruthin, oriciacridon, and 5-hydroxynoracronycin in 36-month-old roots. These findings highlight the dual benefits of gamma-assisted CeO_2/SiO_2 synthesis and its effectiveness in simultaneously increasing biomass production and phytochemical quality, offering a sustainable nanotechnology-based approach for cultivating medicinal plants.

1 | Introduction

Among the imported medicinal plants, *Salvia miltiorrhiza* Bunge (denoted as SMB), belonging to the genus *Salvia* in the Lamiaceae family, is recognized as an essential herb widely used as an ancient medicine in several Asian countries. To date, more than 20 phenolic acids isolated from the roots of SMB have been studied. These substances comprise oil-soluble tanshinone diterpenoids, such as tanshinone I, tanshinone IIA, and cryptotanshinone. Over 30 tanshinones and quinone diterpenoids have been isolated and synthesized [1, 2].

Paramignya trimera (Oliv.) Guillaum (denoted as PTG) belongs to the Rutaceae family and is mainly distributed in southern Vietnam. PTG is a woody plant characterized by thorns located in the leaf axils. Studies on PTG, encompassing its stem, roots, and leaves, reveal that the primary chemical components consist of coumarins, alkaloids, flavonoids, and organic acids. These

compounds demonstrate α-glucosidase inhibitory activity, with IC50 values ranging from 14.6 to 112.2 μM, which are stronger than the positive control, acarbose (IC50, 214.5 μM) [1, 3]. Silicon dioxide nanoparticles (SiO_2 NPs) have multifunctional applications [2], particularly in biomedical sciences [4], agriculture [5], industry [2], cosmetics [6], medicine [7], and others. Given the high medicinal and economic value of SMB and PTG, the development of advanced cultivation strategies, particularly through nanotechnology-based nutrient delivery systems, has become an important research direction to enhance their growth performance and bioactive compound accumulation. SiO_2 NPs play a significant role in supplying silicon to plants in agriculture. Silicon influences and promotes crop growth, especially in challenging conditions. It is widely recognized as a beneficial element for crops [8, 9]. In plants, silicon is primarily accumulated in the cell walls [10, 11], thus strengthening them, increasing mechanical resilience, and mitigating various biotic and abiotic stresses [12, 13].

Experiments have shown increases of over 10% in rice, even under severe leaf blast conditions [14, 15]. However, nanosilica materials have limitations in stimulating root system development and antiviral capabilities. Cerium oxide nanoparticles (CeO_2 NPs) are among the 13 rare earth oxide nanoparticles with diverse industrial applications and are extensively studied in agriculture [16, 17]. CeO_2 NPs have been reported to impact crop yield [18, 19] and can modify the nutritional profile of plants [20, 21], as they stimulate plant growth at low concentrations [21] in lettuce (*Lactuca sativa* L.). The application of CeO_2 NPs at 100 mg kg^{-1} improved Rubisco activity, water use efficiency, and light absorption rates in soybeans [22], and similar benefits of CeO_2 NPs on tomato yield [20] and wheat growth [21] have also been observed. Another benefit of CeO_2 is its antibacterial and antifungal properties [23, 24]. However, due to its high cost, CeO_2 is not a conventional metal for addressing bacterial and viral resistance in crops [25]. The combination of CeO_2/SiO_2 NPs presents an effective solution to overcome the limitations of single materials. Nanocomposite materials have been synthesized using various approaches, including chemical precipitation [26], gel formation [27], hydrothermal method [28], spray hydrolysis [29], and continuous hydrothermal synthesis [30]. Although these techniques are well established, some are mainly suitable for laboratory-scale production, while others are designed for large-scale manufacturing and typically require high temperatures, complex reactor systems, and substantial energy input, which increase operational costs. Moreover, under rapid thermal or continuous-flow conditions, achieving uniform dispersion and controlled deposition of CeO_2 nanoparticles on a SiO_2 matrix remains challenging. In contrast, gamma irradiation-assisted synthesis provides a mild and low-temperature alternative that enables homogeneous nucleation and controlled nanoparticle growth without the need for high-pressure or high-temperature equipment. This approach relies on the in situ generation of reactive species, allowing nanoparticle formation and integration under ambient conditions. Compared with conventional chemical or thermal methods, irradiation offers improved control over particle size and dispersion, eliminates the use of toxic reagents, and reduces secondary by-products [31]. Furthermore, the irradiation dose can be precisely regulated, ensuring high reproducibility and scalability [32].

Therefore, the development of an efficient and scalable route for producing CeO_2/SiO_2 nanocomposites using Co-60 gamma irradiation is of considerable interest. In this work, we propose a straightforward and cost-effective strategy for synthesizing CeO_2/SiO_2 nanoparticles derived from rice husk-based SiO_2 and cerium salt under gamma irradiation.

Proper nutrient management strategies are crucial for improving the medicinal quality and maximizing the yield of SMB and PTG plants. Traditionally, these medicinal species have mostly depended on natural growing conditions, as they are usually suited to temperate or semitropical environments. In this study, cultivation shifted from natural habitats to controlled artificial settings. A new CeO_2/SiO_2-based fertilizer was used as a nutritional supplement to support the growth and bioactive potential of SMB and PTG plants.

2 | Materials and Methods

2.1 | Materials

Nanosilica (SiO_2 NPs) was derived from rice husk using the hydrothermal method. Cerium(III) nitrate hexahydrate (99.5%) was purchased from Fujifilm Wako Chemical (USA). Chitosan was obtained from Chitosan Vietnam (Vietnam). Other chemicals were of analytical grade (Merck).

2.2 | Synthesis of Nano SiO_2/CeO_2 Composite

Rice husk ash was collected as a crude sample from the process of burning rice husk to generate heat for a small local factory. The rice husk ash was treated with tap water in a plastic basin at a solid-to-liquid ratio of 1:5 (kg L^{-1}) and stirred for 1 h at room temperature. The mixture was then filtered and washed with distilled water. After treatment with distilled water, the rice husk ash underwent two treatments with a 5% HCl solution in a 1-L glass beaker at a solid-to-liquid ratio of 1:1 (kg L^{-1}), stirred on a magnetic stirrer and heated for 2 h at 70°C. The treated solid was filtered and washed with distilled water until reaching a neutral pH, which resulted in wet ash. This step aims to completely separate metals or metal ions from the rice husk ash. The wet ash was dried at 120°C for 3 h to obtain dry ash. Next, it was finely ground and calcined at 650°C; the resulting product, a clean and dry ash, was used for subsequent experiments. The ash was dissolved in an alkaline KOH solution in a Teflon bottle. The ash mixture was stirred with a 6 M KOH solution in a ratio of 30 g of ash to 100 mL of KOH. The mixture was placed in a Teflon bottle and it was heated to 180°C for 3 h, and then the suspension was filtered to obtain the solution. The solution was neutralized with hydrochloric acid (HCl) to yield silicic acid precipitate. The precipitate was washed with 5% HCl and then filtered to obtain $SiO_2.nH_2O$. The $SiO_2.2\,H_2O$ precipitate was calcinated at 650°C for 4 h; the resulting product was pure nanosilica (SiO_2) [33].

The CeO_2 NPs and CeO_2/SiO_2 NPs were produced following the Co-60 gamma irradiation process, as follows: $Ce(NO_3)_3.6\,H_2O$ (9 g) was dispersed in 60 mL of water with or without 2.0 g of SiO_2 NPs. These solutions were combined by dispersion in a 2% chitosan solution, resulting in a total volume of 5 L. They were then subjected to Co-60 gamma irradiation with a dose of 25 kGy to produce CeO_2 and CeO_2/SiO_2, respectively. Finally, the

resulting suspensions were cooled to room temperature in a vacuum box and then stored in PE bottles. The pH of the chitosan solution was 4.5–5.0, and after irradiation, the pH was adjusted to 6.5–7.0.

Scheme 1 depicts the CeO_2/SiO_2 preparation device. At this capacity, we can produce 1 ton of product daily. A brief schematic overview is shown in Scheme 2. The Co-60 radioactive source is safely stored in a water pool (1.5–2 m deep) to provide radiation shielding when not in use. During irradiation, the source is lifted from the rack to emit gamma rays. Samples are placed in product carriers and moved into the irradiation chamber via a sealed conveyor system, preventing radiation leakage. After the designated irradiation period, the conveyor transports the products out of the chamber, while the process is monitored by a control and safety system. The irradiated products are sterilized or surface-modified according to research goals and are not radioactive, so they can be used immediately after quality inspection. The parameters are as follows: dose rate: 5 kGy/h; duration: 5 h; system includes isotope: Co-60; gamma-ray energy: 1.17 MeV; half-life: 5.27 years; industrial dose rate: 5–30 kGy/h; and working dose ranges: low: 0.1–1 kGy; medium: 1–10 kGy; high: 10–50 kGy; and very high: > 100 kGy.

2.3 | Characterization

The structure and morphology of the resulting materials were characterized using x-ray diffraction (XRD, Bruker D8 Advance) and scanning electron microscopy (SEM, JEOL JSM-7610F). EDX mapping was conducted with Hitachi S-4800 FESEM (Japan). Nitrogen adsorption/desorption isotherms were measured on a Micromeritics Tristar-3030 system (USA). High-resolution electron microscopy was performed with a JEM 1010 transmission electron microscope (JEOL, Japan; 80 kV). Fourier transform infrared (FTIR) spectroscopy was conducted using a Spectrum 1000 Perkin-Elmer spectrometer. Chlorophyll b content was determined by the spectrophotometric method [34] using a Uviline 9400 instrument and a Specord 50 UV–Vis spectrophotometer (Analytik Jena AG, Germany) at the wavelengths of 645 and 663 nm. All measurements were conducted in triplicate.

2.4 | The Preparation of SMB and PTG

This section describes the preparation, propagation, and field cultivation procedures for SMB and PTG, including seed and cutting pretreatments, planting substrates, experimental design, and nanoparticle application regimes used in this study.

2.4.1 | Growing SMB From Seeds

SMB seeds were purchased from the Institute of Medicinal Materials (Vietnam), soaked in a 4 mg L^{-1} CeO_2/SiO_2 NP suspension for 30 min, removed, drained in a cloth bag for 24 h, and then planted in the experimental garden.

Preparing the planting soil: including light loam, coconut fiber, burnt rice husks, and composted manure.

2.4.2 | Growing PTG by Cuttings

Choosing the parent plant for propagation: the parent plant used for propagation must be healthy, free of pathogens and dangerous insects. The length of the cutting should be about 5–20 cm. CeO_2/SiO_2 NPs were dispersed in a nanochitosan solution at a concentration of 40 mg L^{-1} to stimulate the rooting of cuttings. The cutting substrate was used to fix the cuttings, maintain moisture, provide air circulation, and shade the bottom of the cuttings; commonly used substrates are humus, coconut fiber, and burnt rice husks. The rooting time is about 45–50 days, and the rooting rate is about 80%–90%. After rooting, the cuttings were planted in cellulose pots containing light loam, coconut fiber, burnt rice husks, and composted manure. The seedlings were kept in a cool place and watered regularly. Watering was performed 1-2 times a day in the early morning and/or late afternoon. After 90 days, the plants were brought to the garden for planted.

The area testing was located in Binh Dinh Province, Vietnam. The area of each trial plot was at least 100 m^2, with a planting density of 1000 plants ha^{-1}. Each experimental treatment was repeated at least 3 times, and the area for each experimental treatment was 100 m^2. In this study, the research time was 12 months for testing. The research formulas in the trial are as follows:

Treatment 1: 0.5 g of CeO_2/SiO_2 NPs was dispersed homogeneously in 1 L of soluble-water chitosan (0.5 g L^{-1}) to obtain a CeO_2/SiO_2/chitosan suspension. This solution, with different volumes, e.g., 1 L, 1.5 L, 2 L, 2.5 L, and 2.5 L diluted with 360 L of water, was used to spray plants at various times: the first month, third month, sixth month, ninth month, and 20th month,

SCHEME 1 | Image of C-60 gamma ray generator.

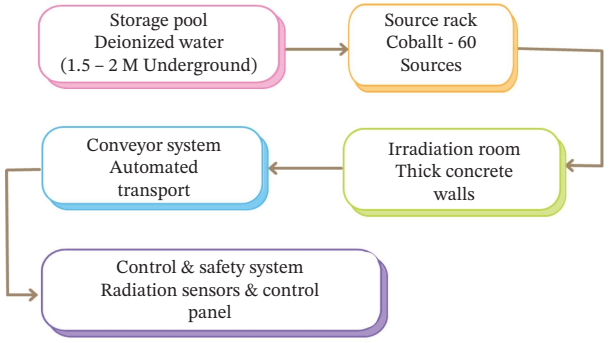

SCHEME 2 | Co-60 irradiation system.

respectively. The estimated application rate of the nanocomposite is approximately 1 g ha^{-1}.

Treatment 2: similar to Treatment 1, except that 0.5 g of CeO_2/SiO_2 NPs was replaced with 1.0 g of CeO_2/SiO_2 NPs.

Treatment 3: similar to Treatment 1, except that 0.5 g of CeO_2/SiO_2 NPs was replaced with 1.5 g of CeO_2/SiO_2 NPs.

Treatment 4: similar to Treatment 1, except that 0.5 g of CeO_2/SiO_2 NPs was replaced with 2.0 g of CeO_2/SiO_2 NPs.

Treatment 5: similar to Treatment 1, except that 0.5 g of CeO_2/SiO_2 NPs was replaced with 2.5 g of CeO_2/SiO_2 NPs.

Control formula: similar to Treatment 1, except that 0.5 g of CeO_2/SiO_2 NPs was replaced with 0.0 g of CeO_2/SiO_2 NPs.

3 | Results and Discussion

3.1 | Characterization of Materials

Figure 1a presents the XRD pattern of SiO_2. A broad diffraction peak appeared at around the 2 theta of 23^0 is typical of amorphous in nature. Meanwhile, on the XRD pattern of CeO_2, firm diffraction peaks are observed at 2 theta of 29, 33, 47, and 56^0, corresponding to the (401), (300), (400), and (622) planes of CeO_2, respectively (according to JCPDS 04-0856) (Figure 1a). The XRD patterns of the CeO_2/SiO_2 materials exhibited characteristic diffraction peaks of CeO_2 with weak magnitudes due to the amorphous nature of SiO_2. This result confirms the formation of SiO_2/CeO_2 composite. Figure 1b exhibits the FT-IR spectra of the CeO_2, SiO_2, and CeO_2/SiO_2 materials. The peaks assigned to the −OH vibration of water molecules appeared at 3412–3456 cm^{-1} and 1630 cm^{-1}. The peaks at about 887 and 725 cm^{-1} wavenumbers in CeO_2 spectrum were assigned to −O−Ce stretch of CeO_2 [33]. The peaks at about 1100 and 947 cm^{-1} wavenumbers were assigned to Si−O−Si asymmetric and symmetric stretching vibrations, respectively. The small peak at about 486 cm^{-1} indicated the bending vibration of O−Si−O [35]. On the other hand, the FT-IR spectrum of CeO_2/SiO_2 exhibits peaks assigned to Si-O stretching at approximately 1103 cm^{-1}. The 469 and 725 cm^{-1} peaks were assigned to the Si-O and Ce−O stretching of CeO_2/SiO_2, respectively. The results confirmed the formation of CeO_2/SiO_2 composite. The nitrogen adsorption/desorption isotherms on SiO_2, CeO_2, and CeO_2/SiO_2 materials are shown in Figure 1c. N_2 adsorption−desorption curves were classified as Type II, according to IUPAC, indicating that the samples contain both porous and nonporous structures (Figure 1c). The specific surface areas of 43, 20, and 26 $m^2 g^{-1}$ were obtained for SiO_2, CeO_2, and CeO_2/SiO_2, respectively. Although SiO_2, CeO_2, and the CeO_2/SiO_2 composite exhibit similar adsorption–desorption isotherms, their specific surface areas differ significantly. The intermediate surface area of the composite indicates partial pore coverage by CeO_2 nanoparticles on the SiO_2 surface, while maintaining a mesoporous structure.

To determine the elemental composition present in the CeO_2/SiO_2 material, the materials were characterized using energy-dispersive x-ray spectroscopy mapping. Figure 2b shows that the sample contains only Si, Ce, and O as expected. The peaks with strong intensity characteristic of Si, O, and Ce appear at energy levels of 1.88, 0.50, and 0.93 keV, respectively. The initial molar Ce/Si ratio of 0.62 is close to the EDX Ce/Si ratio of 0.68, and the result of EDX spectrum mapping reveals that these elements are evenly dispersed among each other.

The morphology of CeO_2, SiO_2, and CeO_2/SiO_2 materials was examined using the SEM method, with results as shown in Figure 3. The SEM images in Figure 3 show that the CeO_2 material consists of very fine particles with various shapes that tend to agglomerate. Similarly, the SiO_2 material comprises aggregated particles, resulting in a rough and uneven surface. In the case of CeO_2/SiO_2 material, the dispersion of CeO_2 particles is distributed on SiO_2, creating a similarly rough and uneven surface.

The HRTEM images of SiO_2, CeO_2, and CeO_2/SiO_2 materials dispersed in 2% chitosan are shown in Figure 4. The SiO_2 and CeO_2 materials had a mean size of about 8.7 ± 3.9 nm and 5.2 ± 2.7 nm (Figure 4a, b), while the average size distribution of CeO_2/SiO_2 was 12.6 ± 2.5 nm (Figure 4c). These results indicate that the Co-60 gamma irradiation-assisted method can synthesize materials with high dispersion at a size of several nanometers. In addition, using this method, we can synthesize large amounts for practical use; this is an excellent advantage over methods such as sol-gel or hydrothermal processes.

3.2 | Using CeO_2/SiO_2 NPs as Nanofertilizer for SMB

The influence of CeO_2/SiO_2 NPs on the germination of SMB and the shoot height after 2 weeks of cultivation was studied (Table 1). In the control group, only 14% of SMB seeds germinated with an average shoot height of 2.0 cm. In contrast, the germination rate of SMB seeds, especially the shoot height, increased significantly as CeO_2/SiO_2 NPs were applied. The highest germination rate (90%) was achieved when supplemented with 1.0 g L^{-1}. The germination rate gradually decreased from 90% to 34% as the nano CeO_2/SiO_2 concentration increased from 1 g L^{-1} to 2 g L^{-1}. A two-way contingency table analysis was performed to evaluate how the different concentrations of CeO_2/SiO_2 NPs affect the germination of SMB. Two variables were evaluated: CeO_2/SiO_2 NPs with five levels, including the control and various concentrations of CeO_2/SiO_2 NPs (0.5, 1, 1.5, and 2 g L^{-1}, and the germination status (germinated and nongerminated) after 2 weeks. The concentration of CeO_2/SiO_2 NPs and germination were significantly related (Pearson chi square $(4, 495) = 174.9$, $p < 0.001$). The germination rate is presented in Table 1. Follow-up pairwise comparisons were performed to assess the difference in germination rate. Table S1 presents the results of these

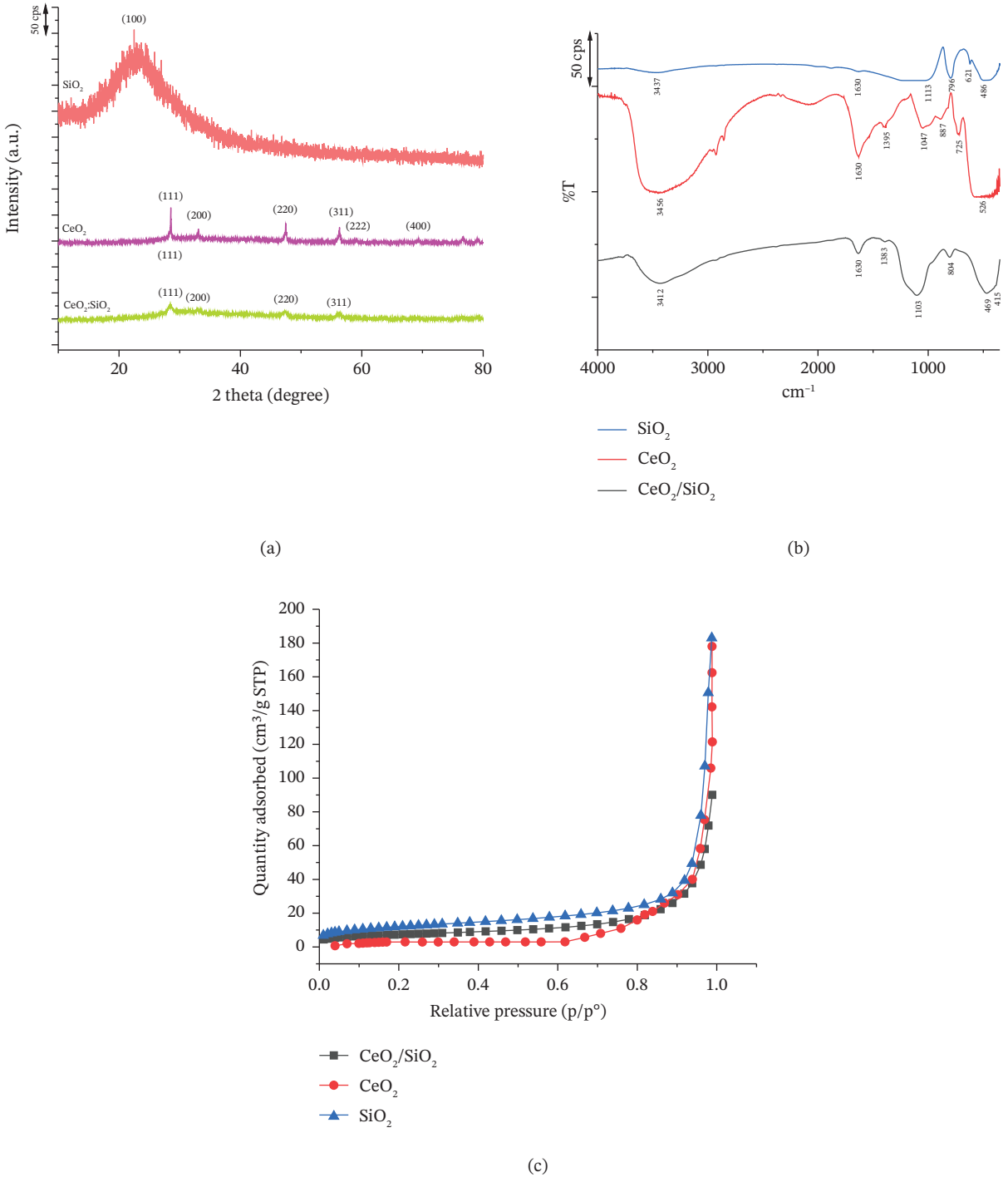

FIGURE 1 | (a) XRD patterns, (b) IR spectra, and (c) N_2 adsorption–desorption isotherms of the CeO_2, SiO_2, and CeO_2/SiO_2 materials.

analyses. Holm's sequential Bonferroni approach was employed to control Type I error at 0.05 level across all three comparisons. The germination proportion applied by the CeO_2/SiO_2 NPs was significantly higher than the control group. The germination proportion (90%) used by the 1 g L^{-1} treatment was significantly higher than the rest. Therefore, the suitable CeO_2/SiO_2 NP concentration for SMB germination is 1.0 mg L^{-1}. It is worth noting that, unlike the germination stimulation ability, the shoot height increased statistically significantly (Tables S2-3) with the concentration of nanofertilizer, so we continued to study the effect of the concentration of CeO_2/SiO_2 NPs on the root system (SMB plants are mainly exploited using the root part) (Table 1). Table 1 shows the development of the root length after 12 months using different treatments. It was found that when CeO_2/SiO_2 nanofertilizer was applied at increasing concentrations, the root growth indices of SMB plants also tended to improve. The root length increased insignificantly at 0.5; 1.0; and 1.5 g L^{-1}. However, at a concentration of 2.0 g L^{-1}, the root length doubled compared to the control sample, indicating a clear effect in stimulating root growth. Notably, when the concentration was increased to 2.5 g L^{-1}, root growth no longer increased, which may induce severe phytotoxicity [36], reflecting nutrient

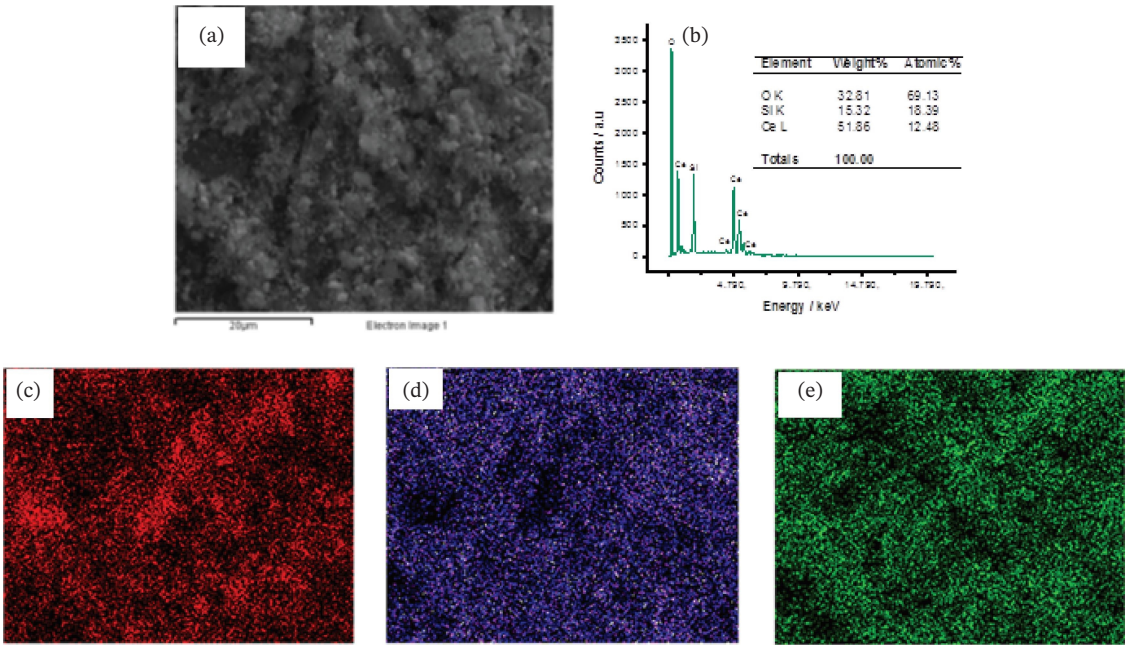

FIGURE 2 | EDX mapping of CeO_2/SiO_2: (a) electron image, (b) EDX spectrum, (c) Si element (d) Ce element, and (e) O element.

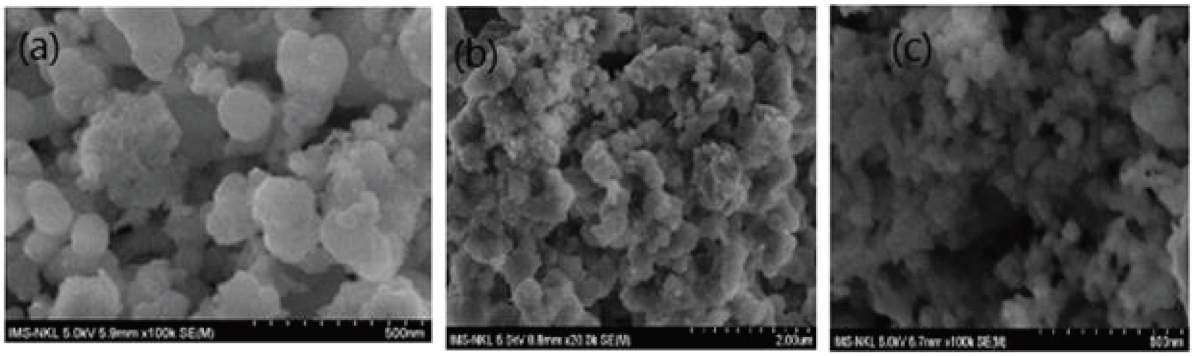

FIGURE 3 | SEM images of SiO_2 (a), CeO_2, (b) and CeO_2/SiO_2 (c).

saturation as the SMB plants' absorption demand reached the maximum threshold. A one-way analysis of variance (ANOVA) was performed to assess the relationship between CeO_2/SiO_2 NP concentration and the development of the root length and the number of roots of 12 old-month plants. The ANOVAs are significant: $F(5,114) = 180.9$, $p < 0.001$ for the root length, and $F(5,114) = 175.4$, $p < 0.001$ for the number of roots per plant. The follow-up tests were performed to evaluate pairwise differences among the means, conducting post hoc comparisons using Turkey's test (Tables S4 and 5). It can be concluded that there is a statistical difference between the control group and the group using CeO_2/SiO_2 NPs in terms of the development of root length and the number of roots. Root length and the number of roots increased significantly as CeO_2/SiO_2 concentration increased, reaching a maximum at 2 g L^{-1}, after which root length growth and the number of roots per plant had no statistical difference as CeO_2/SiO_2 NP concentration increased, The average root lengths using 2 g L^{-1} and 2.5 g L^{-1} were 22.5 and 22.4 cm, respectively ($p = 0.69 > 0.05$). The number of roots using 2 g L^{-1} and 2.5 g L^{-1} was 11.9 and 12.4, respectively ($p = 0.086$). Therefore, 2 g L^{-1} concentration was considered the optimal concentration.

Figures 5a and b illustrate a growing SMB area, as well as the morphology of SMB plants using different treatments.

Evaluation of the photosynthetic capacity of SMB plants when using nanofertilizers. To evaluate the photosynthetic capacity of SMB plants when using nanofertilizers, we selected the criterion of analyzing the chlorophyll b content in the leaves of SMB plants.

Based on Table 2, the analysis of chlorophyll b content shows a significant enhancement in the photosynthetic capacity of SMB plants, with the highest chlorophyll b formation occurring in the 12th month. This can be explained as follows: by the 12th month, the root system of SMB has developed significantly, and fertilization at this stage provides both nutrients and catalytic agents that enhance photosynthesis on the leaf surface of SMP plants. Therefore, the formation of chlorophyll b also increases.

3.3 | Nano CeO_2/SiO_2 Fertilizer for PTG

The growth parameters of PTG planting using nano CeO_2/SiO_2 and the control were measured over a period of 12 months. The growth parameters increased over time from planning to 12

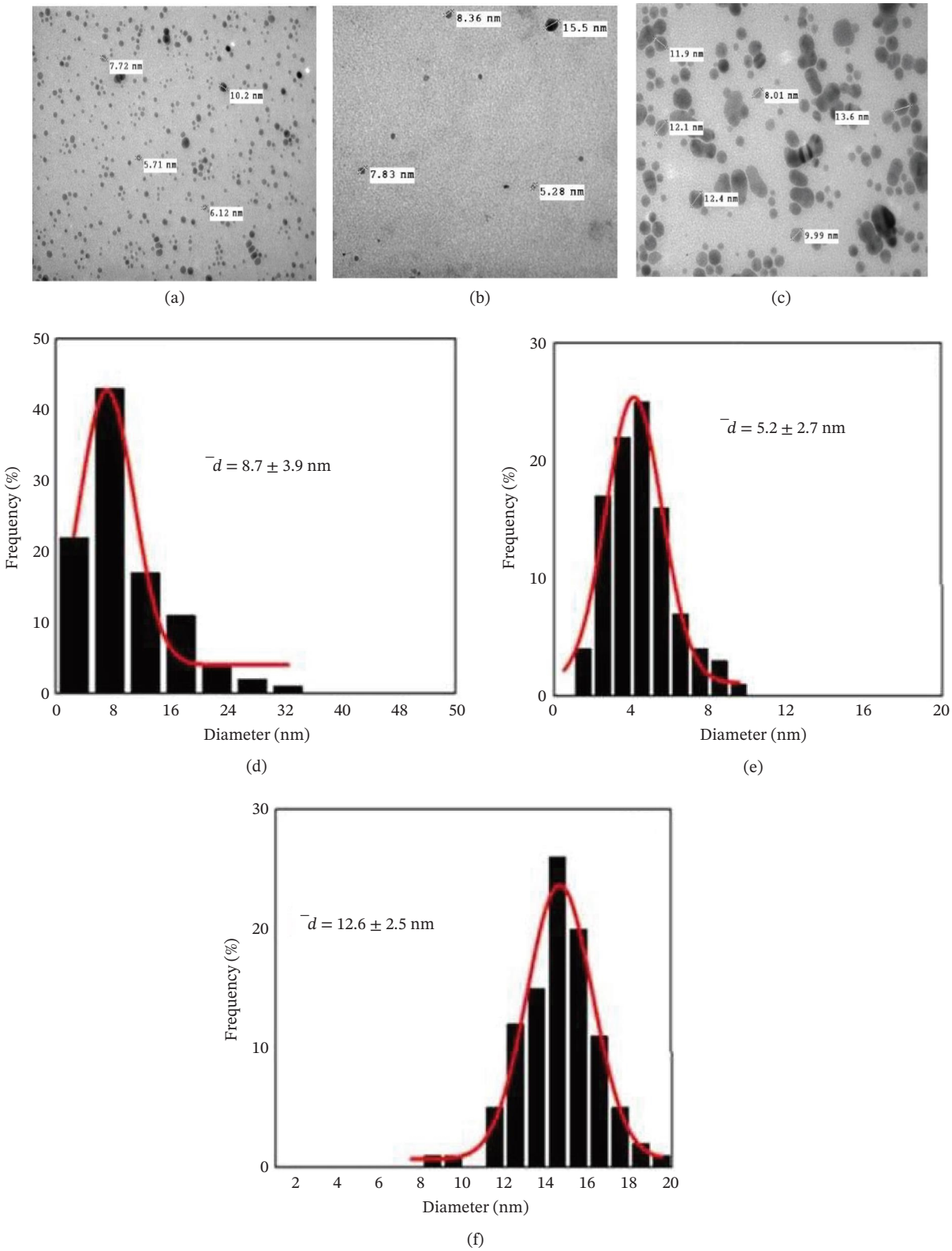

FIGURE 4 | TEM images of SiO_2 (a), CeO_2 (b), and CeO_2/SiO_2 (c) in the chitosan matrix and the corresponding particle size distributions of SiO_2 (d), CeO_2 (e), and CeO_2/SiO_2 (f).

months. The results of measuring the trunk height, leaf length, and root length showed that these parameters of PTG plants increased with increasing concentration of CeO_2/SiO_2. Figure 6 illustrates the development of the trunk height, leaf length, and root length using different treatments of the 12-month-old plants.

A one-way ANOVA was conducted to interpret the effect of the nano CeO_2/SiO_2 fertilizer using five treatments on growth parameters, including trunk height (Table S6-7), leaf length (Table S8-9), and root length (Table S10-11). The results reveal a significant effect: $F(4, 45) = 373.4$, $p < 0.001$ for the trunk

TABLE 1 | Influence of nano CeO_2/SiO_2 NPs on the germination ability of SMB after 2 weeks of cultivation (except the root length of 12 months).

Nano CeO_2/SiO_2 (g L^{-1})	Percentage of seed sprouting (%) ($n = 100$)	Shoot height (cm) ($n = 20$)	Root length after 12 months ($n = 20$)	The number of roots in a plant ($n = 20$)
Control	14	2.0	11.0	5.4
Treatment 1 (0.5)	29	4.8	13.0	5.7
Treatment 2 (1.0)	90	7.6	13.8	6.6
Treatment 3 (1.5)	79	8.7	14.6	7.6
Treatment 4 (2.0)	34	9.5	22.5	11.9
Treatment 5 (2.5)	n/a	n/a	22.4	12.4

(a) (b)

FIGURE 5 | (a) Concentration of CeO_2/SiO_2 NPs: 0.5 g L^{-1}, (b) concentration of CeO_2/SiO_2 NPs: 1.0 g L^{-1}, (c) concentration of CeO_2/SiO_2 NPs: 1.5 g L^{-1}, (d) concentration of CeO_2/SiO_2 NPs: 2.0 g L^{-1}, and (e) control.

TABLE 2 | Evaluation of the photosynthetic capacity of SMB plants.

Evaluation criteria	Units	Time (months)		
		04	08	12
The content of chlorophyll b in the leaves of SMB plants (experimental)	μg g^{-1}	12.2	18.1	26.1
The content of chlorophyll b in the leaves of SMB plants (control)	μg g^{-1}	11.6	15.2	23.1

(a) (b)

FIGURE 6 | (a) The development of trunk height, leaf length, and root length of PTG plants after 12 months under different treatments and (b) roots of 36-month-old PTG plants.

TABLE 3 | Analysis of coumarins in root samples.

No.	Compound name	Concentration (mg kg^{-1}) (experimental sample)	Concentration (mg kg^{-1}) (control sample)
1	Ostruthin	320.132 ± 0.312	132.234 ± 1.013
2	8-Methoxy ostruthin	114.235 ± 0.415	91.261 ± 0.912
3	Oriciacridon	34.323 ± 0.114	17.124 ± 0.818
4	5-Hydroxynoracronycin	36.137 ± 0.222	15.088 ± 0.718

height; $F(4, 45) = 120.1$, $p < 0.001$ for leaf length; and $F(4, 45) = 1400.7$, $p < 0.001$ for root length. Post hoc tests were performed using Tukey's HSD test. The comparison indicates a significant difference between treatments, as shown in Tables S5, S7, and S9. Therefore, the null hypothesis that different concentrations of the nano CeO_2/SiO_2 fertilizer have the same effect on the growth parameters is rejected. The results of post hoc analysis showed that when the concentration increased across 0.0, 0.5, 1, 1,5, and 2 g L^{-1}, the plant growth parameters increased and had statistical differences and reached a maximum at 2 g L^{-1}. When the concentration continued to increase to 2.5 g L^{-1}, the root length and plant height did not change significantly ($p = 0.793$ for root length, $p = 0.083$ for trunk height), while the leaf length decreased significantly. From fertilizer concentrations of 0.5 g L^{-1}–2.0 g L^{-1}, growth parameters improved significantly, possibly due to enhanced root development that facilitated more efficient nutrient uptake. However, at a concentration of 2.5 g L^{-1}, growth plateaued, suggesting that the plants had reached a nutrient absorption saturation point. Notably, a reduction in leaf number was observed at the 2.5 g L^{-1} concentration. This may be explained by the increased absorption of monochromatic light at this level, which could partially disrupt leaf cell structures, thereby limiting leaf development compared to the 2.0 g L^{-1} concentration.

After 12 months of experimenting with the fertilizer for PTG, it can be concluded that the fertilizer for this crop has shown quite positive results. This is evident through parameters such as plant height, leaf length, and root length, which developed in a linear ratio with fertilizer concentration and the study parameters. Thus, it can be confirmed that this fertilizer can be used in the nutrient cycle for PTG and is highly promising for generating yields for this valuable medicinal plant.

Roots of 36-month-old PTG were collected from the cultivation site, air-dried, and ground into powder. The powder (500 g) was then extracted sequentially with n-hexane followed by ethyl acetate (EtOAc) using a Soxhlet extractor. After solvent removal, 11.5 g of n-hexane extract and 4.5 g of EtOAc extract were obtained. Column chromatography (CC) of the n-hexane extract on silica gel (eluted with hexane–EtOAc, 0%–100%) yielded five fractions (H1–H5). Further CC of 2.1 g of fraction H2 on silica gel (eluted with hexane–EtOAc, 0%–100%, followed by $CHCl_3$–MeOH, 0%–5%) was performed. The analytical results are presented in Table 3.

The results presented in Table 3 show that the concentrations of ostruthin, 8-methoxy ostruthin, oriciacridon, and 5-hydroxynoracronycin in the roots of 36-month-old *Paramignya trimera* plants in the experimental group were significantly higher than those in the control group. Notably, the ostruthin concentration in the experimental samples was twice as high as that in the control samples.

The present work primarily focused on evaluating agronomic outcomes rather than mechanistic pathways; however, the observed responses are in agreement with previously proposed mechanisms. Accordingly, CeO_2 nanoparticles exhibit reversible Ce^{3+}/Ce^{4+} redox cycling, enabling ROS scavenging and nanozyme-like antioxidant activity that protects photosynthetic structures and increases chlorophyll accumulation [37]. SiO_2 supplies bioavailable silicon that strengthens cell walls and boosts stress tolerance and nutrient absorption [38]. Additionally, chitosan functions as an elicitor that triggers plant defense signaling and the production of secondary metabolites [39, 40]. The combined action of these components probably explains the improved germination, growth, and phytochemical accumulation seen in SMB and PTG.

4 | Conclusions

CeO_2/SiO_2 nanoparticles were synthesized from rice husks and $Ce(NO_3)_3$ via a high-efficiency Co-60 gamma irradiation process, enabling large-scale production at a capacity of up to one ton per hour. Structural analysis revealed that the synthesized material has nanoscale dimensions (12.6 ± 2.5 nm). When used as a growth stimulant for SMB, CeO_2/SiO_2 nanoparticles showed pronounced effectiveness during the germination phase, with the highest germination rate (90%) observed at a concentration of 1.0 g L^{-1}. The study also found that the optimal concentration of CeO_2/SiO_2 nanoparticles for promoting root development in both *Salvia miltiorrhiza* and *Paramignya trimera* is 2.0 g L^{-1}. At a higher concentration of 2.5 g L^{-1}, a significant reduction in leaf number occurred, suggesting that nutrient absorption had reached a saturation threshold. Notably, long-term application of CeO_2/SiO_2 nanoparticles as a fertilizer for *Paramignya trimera* over a 3-year cultivation period resulted in a significant increase in the content of bioactive compounds, including ostruthin, 8-methoxy ostruthin, oriciacridon, and 5-hydroxynoracronycin, in the roots compared to the control group. These findings highlight the potential of CeO_2/SiO_2 nanoparticles as an effective nanofertilizer for the enhanced cultivation of medicinal plants.

Author Contributions

The authors confirm their contributions to the paper: C.V.H, N.V.N.M, L.T.T.N, and D.Q.K contributed to the study conception and final manuscript preparation; N.H.P, N.T.T.P, D.T.N.H, N.T.D.C, and N.V.T collected the data; V.V.D.E, N.C.B, H.V.M.H, L.T.T.N, and L.H.H analyzed and interpreted the results.

Acknowledgments

The authors did not use any AI software to prepare the manuscript.

Funding

This research was supported by the Vietnam Ministry of Education and Training, No. CT2022.08.QNU.05, and partially supported by Hue University under the Core Research Program No. NCTB.DHH.2025.05.

Disclosure

All authors reviewed the results and approved the final version of the manuscript.

Conflicts of Interest

The authors declare no conflicts of interest.

Data Availability Statement

The data used to support the findings of this study are available from the corresponding author upon request.

References

1. D. Q. Tuan, H. V. Duc, L. T. Nhan, L. T. Anh, N. T. Hoai, and A. Raal, "Constituents of Essential Oils From the Leaves of Paramignya Trimera (Oliv.) Guillaum From Vietnam," *Journal of Essential Oil Bearing Plants* 22, no. 2 (2019): 391–395, https://doi.org/10.1080/0972060X.2019.1582362.

2. P. Aggarwal, R. P. Singh, and Y. Aggarwal, "Use of Nano-Silica in Cement Based materials—A Review," *Cogent Engineering* 2, no. 1 (2015): 1078018, https://doi.org/10.1080/23311916.2015.1078018.

3. P. H. Dang, T. H. Le, P. K. T. Phan, P. T. T. Le, M. T. T. Nguyen, and N. T. Nguyen, "Two Acridones and Two Coumarins From the Roots of Paramignya Trimera," *Tetrahedron Letters* 58, no. 16 (2017): 1553–1557, https://doi.org/10.1016/j.tetlet.2017.02.083.

4. Y. Huang, P. Li, R. Zhao, et al., "Silica Nanoparticles: Biomedical Applications and Toxicity," *Biomedicine & Pharmacotherapy* 151 (2022): 113053, https://doi.org/10.1016/j.biopha.2022.113053.

5. S. J. L. Petitjean, M. Lecocq, C. Lelong, et al., "Salvia miltiorrhiza Bunge as a Potential Natural Compound Against COVID-19," *Cells* 11, no. 8 (2022): 1311, https://doi.org/10.3390/cells11081311.

6. S. Nafisi and H. I. Maibach, "Silica Nanoparticles for Increased Cosmetic Ingredient Efficacy⁎," *Cosmetics & Toiletries* (2015).

7. J. Lu, M. Liong, J. I. Zink, and F. Tamanoi, "Mesoporous Silica Nanoparticles as a Delivery System for Hydrophobic Anticancer Drugs," *Small* 3, no. 8 (2007): 1341–1346, https://doi.org/10.1002/smll.200700005.

8. Y. Liang, M. Nikolic, R. Bélanger, et al., "History and Introduction of Silicon Research," *Silicon Agric. From Theory to Pract.* (2015): 1–18, https://doi.org/10.1007/978-94-017-9978-2_1.

9. P. Goswami, J. Mathur, and N. Srivastava, "Silica Nanoparticles as Novel Sustainable Approach for Plant Growth and Crop Protection," *Heliyon* 8, no. 7 (2022): 09908, https://doi.org/10.1016/j.heliyon.2022.e09908.

10. N. Zexer, S. Diehn, and R. Elbaum, "Deposition of Silica in Sorghum Root Endodermis Modifies the Chemistry of Associated Lignin," *Frontiers of Plant Science* 15 (2024): 1370479, https://doi.org/10.3389/fpls.2024.1370479.

11. R. R. Rivai, T. Miyamoto, T. Awano, et al., "Limiting Silicon Supply Alters Lignin Content and Structures of Sorghum Seedling Cell Walls," *Plant Science* 321 (2022): 111325, https://doi.org/10.1016/j.plantsci.2022.111325.

12. K. Radotić, D. Djikanović, A. Kalauzi, G. Tanasijević, V. Maksimović, and J. Dragišić Maksimović, "Influence of Silicon on Polymerization Process During Lignin Synthesis. Implications for Cell Wall Properties," *International Journal of Biological Macromolecules* 198 (2022): 168–174, https://doi.org/10.1016/j.ijbiomac.2021.12.143.

13. M. Pan, X. Gan, C. Mei, and Y. Liang, "Structural Analysis and Transformation of Biosilica During Lignocellulose Fractionation of Rice Straw," *Journal of Molecular Structure* 1127 (2017): 575–582, https://doi.org/10.1016/j.molstruc.2016.08.002.

14. S. M. Ramírez-Olvera, L. I. Trejo-Téllez, F. C. Gómez-Merino, L. D. M. Ruíz-Posadas, E. G. Alcántar-González, and C. Saucedo-Veloz, "Silicon Stimulates Plant Growth and Metabolism in Rice Plants Under Conventional and Osmotic Stress Conditions," *Plants* 10, no. 4 (2021): 777, https://doi.org/10.3390/plants10040777.

15. T. Singh, P. Singh, and A. Singh, "Silicon Significance in Crop Production: Special Consideration to Rice: An Overview," *The Pharma Innovation* 10, no. 3 (2021): 223–229, https://doi.org/10.22271/tpi.2021.v10.i3d.5776.

16. M. Perullini, S. A. Aldabe Bilmes, and M. Jobbágy, "Cerium Oxide Nanoparticles: Structure, Applications, Reactivity, and Eco-Toxicology, Nanomater. a Danger or a Promise?" *A Chem. Biol. Perspect.* (2013): 307–333, https://doi.org/10.1007/978-1-4471-4213-3.

17. H. R. Ahmad, M. Zia-ur-Rehman, M. I. Sohail, et al., *Chapter 11-Effects of Rare Earth Oxide Nanoparticles on Plants* (Academic Press, 2018), 239–275, https://doi.org/10.1016/B978-0-12-811487-2.00011-6.

18. C. M. Rico, S. C. Lee, R. Rubenecia, et al., "Cerium Oxide Nanoparticles Impact Yield and Modify Nutritional Parameters in Wheat (Triticum aestivum L.)," *Journal of Agricultural and Food Chemistry* 62, no. 40 (2014): 9669–9675, https://doi.org/10.1021/jf503526r.

19. Q. Wang, X. Ma, W. Zhang, H. Pei, and Y. Chen, "The Impact of Cerium Oxide Nanoparticles on Tomato (Solanum lycopersicum L.) and its Implications for Food Safety," *Metallomics* 4, no. 10 (2012): 1105–1112, https://doi.org/10.1039/c2mt20149f.

20. W. Du, J. L. Gardea-Torresdey, R. Ji, et al., "Physiological and Biochemical Changes Imposed by CeO_2 Nanoparticles on Wheat: A Life Cycle Field Study," *Environmental Science and Technology* 49, no. 19 (2015): 11884–11893, https://doi.org/10.1021/acs.est.5b03055.

21. W. Du, W. Tan, J. R. Peralta-Videa, et al., "Interaction of Metal Oxide Nanoparticles with Higher Terrestrial Plants: Physiological and Biochemical Aspects," *Plant Physiology and Biochemistry* 110 (2017): 210–225, https://doi.org/10.1016/j.plaphy.2016.04.024.

22. X. Gui, Z. Zhang, S. Liu, et al., "Fate and Phytotoxicity of CeO_2 Nanoparticles on Lettuce Cultured in the Potting Soil Environment," *PLoS One* 10, no. 8 (2015): 0134261, https://doi.org/10.1371/journal.pone.0134261.

23. Y. Li, W. Zhang, J. Niu, and Y. Chen, "Mechanism of Photogenerated Reactive Oxygen Species and Correlation With the Antibacterial Properties of Engineered Metal-Oxide Nanoparticles," *ACS Nano* 6, no. 6 (2012): 5164–5173, https://doi.org/10.1021/nn300934k.

24. D. M. Aruguete, B. Kim, M. F. Hochella, et al., "Antimicrobial Nanotechnology: Its Potential for the Effective Management of Microbial Drug Resistance and Implications for Research Needs in Microbial Nanotoxicology," *Environmental Science: Processes & Impacts* 15, no. 1 (2013): 93–102, https://doi.org/10.1039/C2EM30692A.

25. X. Zhao, R. Long, Y. Chen, and Z. Chen, "Synthesis, Characterization of CeO_2@SiO_2 Nanoparticles and Their Oxide CMP Behavior," *Microelectronic Engineering* 87, no. 9 (2010): 1716–1720, https://doi.org/10.1016/j.mee.2009.09.012.

26. G. Sabeena, E. Pushpalakshmi, S. Rajaduraipandian, and G. Annadurai, "Novel Super Nanocomposite (CeO-SiO_2 Nanocomposite) With Enhanced Biological Application: Synthesis and Characterization," *Plant Nano Biol* 3 (2023): 100025, https://doi.org/10.1016/j.plana.2023.100025.

27. N. Rani, R. Ahlawat, and B. Goswami, "Annealing Effect on Bandgap Energy and Photocatalytic Properties of CeO_2–SiO_2 Nanocomposite Prepared by Sol-Gel Technique," *Materials Chemistry and Physics* 241 (2020): 122401, https://doi.org/10.1016/j.matchemphys.2019.122401.

28. S. Gu, J. Zhou, C. Yu, Z. Luo, Q. Wang, and Z. Shi, "A Novel Two-Staged Thermal Synthesis Method of Generating Nanosilica from Rice Husk via Pre-pyrolysis Combined with Calcination," *Industrial Crops & Products* 65 (2015): 1–6, https://doi.org/10.1016/j.indcrop.2014.11.045.

29. A. K. Bhosale, P. S. Shinde, N. L. Tarwal, P. M. Kadam, S. S. Mali, and P. S. Patil, "Synthesis and Characterization of Spray Pyrolyzed Nanocrystalline CeO_2–SiO_2 Thin Films as Passive Counter Electrodes," *Solar Energy Materials & Solar Cells* 94, no. 5 (2010): 781–787, https://doi.org/10.1016/j.solmat.2009.12.024.

30. U. Alli, S. J. Hettiarachchi, and S. Kellici, "Chemical Functionalisation of 2D Materials by Batch and Continuous Hydrothermal Flow Synthesis," *Chemistry- A European Journal* 29 (2020): 6447–6460, https://doi.org/10.1002/chem.202000383.

31. R. Bisht, G. C. Joshi, J. P. Singh, and C. S. Joshi, "Investigation of the Effect of Gamma-Ray Irradiation on SnO_2 Nanoparticles for Photocatalysis Application," *Nuclear Instruments and Methods in Physics Research Section B: Beam Interactions With Materials and Atoms* 568 (2025): 165862, https://doi.org/10.1016/j.nimb.2025.165862.

32. R. S. Abdelkader, G. A. Helal, Y. G. M. Galal, S. M. Soliman, R. R. Khalil, and N. Elsayed, "New Trends in Mycosynthesis of Cellulose Nanocrystals Promoted by Gamma Irradiation of Sugarcane Bagasse," *International Journal of Environmental Science and Technology* 22, no. 9 (2025): 7867–7884, https://doi.org/10.1007/s13762-024-06144-z.

33. S. Mittal and A. K. Pandey, "Cerium Oxide Nanoparticles Induced Toxicity in Human Lung Cells: Role of ROS Mediated DNA Damage and Apoptosis," *Biomed Research International* 2014, no. 1 (2014): 891934, https://doi.org/10.1155/2014/891934.

34. R. J. Porra, "The Chequered History of the Development and Use of Simultaneous Equations for the Accurate Determination of Chlorophylls a and B," *Photosynthesis Research* 73, no. 1 (2002): 149–156, https://doi.org/10.1023/A:1020470224740.

35. B. Shokri, M. A. Firouzjah, and S. I. Hosseini, "FTIR Analysis of Silicon Dioxide Thin Film Deposited by Metal Organic-based PECVD," *Proceedings of 19th International Symposium on Plasma Chemistry Society* 2631 (2009): 26–31.

36. D. K. Verma, S. Patel, and K. S. Kushwah, "Effects of Nanoparticles on Seed Germination, Growth, Phytotoxicity and Crop Improvement," *Agricultural Reviews* no. 1 (2021): 1, https://doi.org/10.18805/ag.R-1964.

37. M. Pietrzak, E. Skiba, and W. M. Wolf, "Root-Applied Cerium Oxide Nanoparticles and Their Specific Effects on Plants: A Review," *International Journal of Molecular Sciences* 25, no. 7 (2024): 4018, https://doi.org/10.3390/ijms25074018.

38. F. Li, Y. Hou, L. Chen, and Y. Qiu, "Advances in Silica Nanoparticles for Agricultural Applications and Biosynthesis," *Advanced Biotech* 2 (2025): 14, https://doi.org/10.1007/s44307-025-00067-7.

39. R. Nandhini, E. Rajeswari, S. Harish, V. Sivakumar, R. Gangai Selvi, and D. Jaya Sundrasharmila, "Role of Chitosan Nanoparticles in Sustainable Plant Disease Management," *Journal of Nanoparticle Research* 13 (2025): 10–1007, https://doi.org/10.1007/s11051-024-06203-z.

40. T. Nandini, C. Sudhalakshmi, K. Sivakumar, E. Parameswari, and C. Thangamani, "A Review-Chitosan Nanoparticles Towards Enhancing Nutrient Use Efficiency in Crops," *International Journal of Biological Macromolecules* 306 (2025): 141433, https://doi.org/10.1016/j.ijbiomac.2025.141433.

Supporting Information

Additional supporting information can be found online in the Supporting Information section. **Supporting Information.** Holm's sequential Bonferroni method was applied to control Type I error for all pairwise comparisons. Tukey's test indicated that the shoot height of *Salvia miltiorrhiza* seedlings after 2 weeks increased significantly as the CeO_2/SiO_2 concentration rose from 0.5 to 2.0 g L^{-1} (Tables S2–S3). After 12 months, both shoot height and root number of *S. miltiorrhiza*, as well as trunk height, leaf length, and root length of *Paramignya trimera*, increased significantly with increasing CeO_2/SiO_2 concentration, reaching a maximum at 2.0 g L^{-1} (Tables S4–S11).